Laser Deposited High Temperature Thin Film Sensors for Gas Turbines

D. Yang*, V. Pankov, L. Zhao**, and P. Patnaik****

* Automotive and Surface Transportation Research Centre, National Research Canada, 800 Collip Circle, London, ON N4G 4X8

** Aerospace Research Center, National Research Council Canada, 1200 Montreal Road, Ottawa, ON K1A 0R6

CANADA

Dongfang.yang@nrc.gc.ca

ABSTRACT

Multilayer thin film thermocouple sensors consisting of a FeCrAlYZr bond layer, an insulating (Al_2O_3) layer, sensing (Pt and Pt-13Rh) layers and a protective (Al_2O_3) layer have been successfully fabricated on Hastelloy X superalloy substrates at relatively low temperatures by Pulsed Laser Deposition (PLD) and patterned using laser micro-machined shadow masks. This "dry" fabrication approach allows for excellent control of the chemical composition and physical characteristics of the constituent layers and their interfaces, thus achieving good adhesion of the layers to the substrate. The results of thermal cyclic durability testing of the fabricated TFTC sensors demonstrated that the proposed PLD-based approach can be used to fabricate sensors that are fully functional at temperatures up to 750°C. Analyses of the sensor performance during durability testing revealed a number of phenomena including: (i) the existence of a threshold temperature below which accurate temperature measurements were achieved; (ii) an abrupt drop in the sensor output occurring when the sensor temperature exceeded the threshold value, with a fast recovery of the sensor output once the temperature was reduced below the threshold level; (iii) sensor "training" capable of increasing the threshold value of the thin film thermocouple through its exposure to above-the-threshold temperatures.

1.0 INTRODUCTION

Accurate measurements of the temperature distributions in hot section components are indispensable for the Prognostic and Health Management (PHM) of gas turbines. In addition, non-intrusive, fast and accurate techniques for real-time measuring temperatures and strain levels in specific locations of gas turbine engine components are required during engine design stage as well as when critical modifications are introduced in the geometry and/or material selection for these components to ensure that temperatures and stresses in these specific locations do not exceed critical levels. Temperature distribution along the surface of engine component during the engine operation is also needed to validate engine thermal flux models which provide input for failure analysis and life time prediction of these components. Conventional "off-the-shelf" wire- and foil-based thermocouples and strain gauges alter air flows and are typically characterized by low accuracy and delayed response due to their relatively large mass/size. In addition, the operating life of wire and foil thermocouples is extremely short due to the difficulty to reliably secure these sensors on the surface of moving engine components and maintain a reliable thermal contact [1-4]. Thin film thermocouple (TFTC) sensors, directly fabricated on the surface of a component, add negligible mass and create little or no disturbance to airflow and therefore can provide more accurate measurements of fast temperature fluctuations. TFTC sensors for real-time monitoring of engine component temperatures are expected to have a much better thermal cyclic durability compared to the wire and foil thermocouples. For testing and thermal flux modelling of gas turbine engines, TFTC sensors offer non-intrusive real-time temperature measurement of gas turbine engine components in critical locations. NASA Lewis Research Center, [1-3, 5] as well as a consortium consisting of major European aerospace companies including Rolls-Royce, Snecma, Turbomeca and MTU [4] have being actively involved in the development of TFTC sensor technology for turbine engine

applications.

The National Research Council of Canada (NRC) started the development of TFTC sensor technology in 2007 [6]. Different physical vapour deposition techniques, included cathodic arc deposition [6], unbalanced magnetron sputtering [7], electron beam physical vapour deposition (EBPVD) [8] and pulsed laser deposition (PLD) [9] were explored for the fabrication of various functional layers of the sensor, with fully operational TFTC sensors being produced by combining PLD and laser micromachining techniques. This paper describes the fabrication and test results of such a multi-layered Pt/Pt-13%Rh S-type TFTC sensor. The findings include real-time electrical response of the sensor during thermal cycling at temperatures up to 900ºC and structural changes occurred in the functional layers of the sensor as a result of durability testing.

2.0 EXPERIMENTAL

The general design of the TFTC sensor is presented in Fig. 1(a). It is based on the S-type thermocouple junction formed between the Pt and Pt-13 wt. % Rh sensing layers. A series of such sensors was fabricated on the surface of rectangular Hastelloy X substrates with dimensions of 60 mm x 20 mm x 3 mm. The FeCrAlYZr bond layer, Al_2O_3 insulation layer, Pt and Pt-13Rh sensing/leadout tracks, and Al_2O_3 protective layer depicted in Fig. 1(b) were produced sequentially by PLD at substrate temperatures not exceeding 600ºC. PLD of the individual layers of the TFTC sensor was carried out in an experimental deposition chamber (PLD-3000, PVD Inc.) instrumented with a pulsed KrF excimer laser (LPX-210i, Lambda Physik, λ = 248 nm). Prior to deposition, the substrates were mechanically polished with SiC paper through multiple steps up to #800 grit, ultrasonically cleaned with acetone and propanol, dried and finally mounted on a substrate holder in the PLD chamber. The deposition process was performed under conditions listed in Table 1. The compositions of the targets used for fabricating the functional layers and the post-deposition heat treatment parameters are also provided in the table. After the FeCrAlYZr bond layer was deposited, a heat treatment of the coated substrates was performed in the PLD chamber at 600ºC for 3.5 h in a 200 mTorr O_2 atmosphere to form a thin layer of a thermally grown oxide (TGO), which improves electrical insulation of the sensing layers from the metallic substrate. Stenciled shadow masks made of nickel foils by the laser micromachining method were placed in front of the substrate during deposition of subsequent Al_2O_3, Pt, Pt-13Rh and Al_2O_3 layers. The Pt sensing/leadout track layer was deposited first, followed by the Pt-13Rh layer. The mask was positioned in a way to provide a small overlapping area between the Pt and Pt-13Rh layers in order to form the thermocouple junction shown in Fig. 1(a). Oxygen gas was introduced to the chamber during deposition of the Al_2O_3 layers, while deposition of the Pt and Pt13Rh layers was carried out under vacuum at a pressure of $< 2 \times 10^{-7}$ Torr.

Durability testing of the TFTC sensor was performed in a split-type tubular furnace (Series 3210, Applied Test Systems Inc.) powered with a temperature control system 15Q. The signal from the sensor was analyzed using a data acquisition system (MW100, Yokogama Electric Corporation). Electrical connections to the sensor were provided using a custom-designed alumina fixture (see Fig. 2) fabricated by Ortech Inc. (Sacramento, CA) equipped with a pair of Pt and Pt-13Rh contacts. An additional S-type wire thermocouple was attached to the back side of the substrate. The wire thermocouple was used as a reference and its signal was also recorded using the same data acquisition system during testing. The experimental setup shown in Fig. 2 was used for preliminary evaluation of functionality and thermal durability of the fabricated sensor prototype. In the case of the TFTC sensor testing in real engine environment, the sensor geometry as well as wiring have to be slightly modified in order to address the shape complexity of the selected engine component to be instrumented by the sensor. The surface morphology of the TFTC sensor after testing was analyzed using a stereo microscope (Nikon SM71000), a metallographic microscope (Olympus PMG-3), a WYKO optical surface profiler, and a scanning electron microscope (SEM, Philips XL30S) in secondary electron (SE) and backscattered electron (BSE) modes. The elemental compositional analysis of the sensor surface was performed by energy dispersive spectroscopy (EDS).

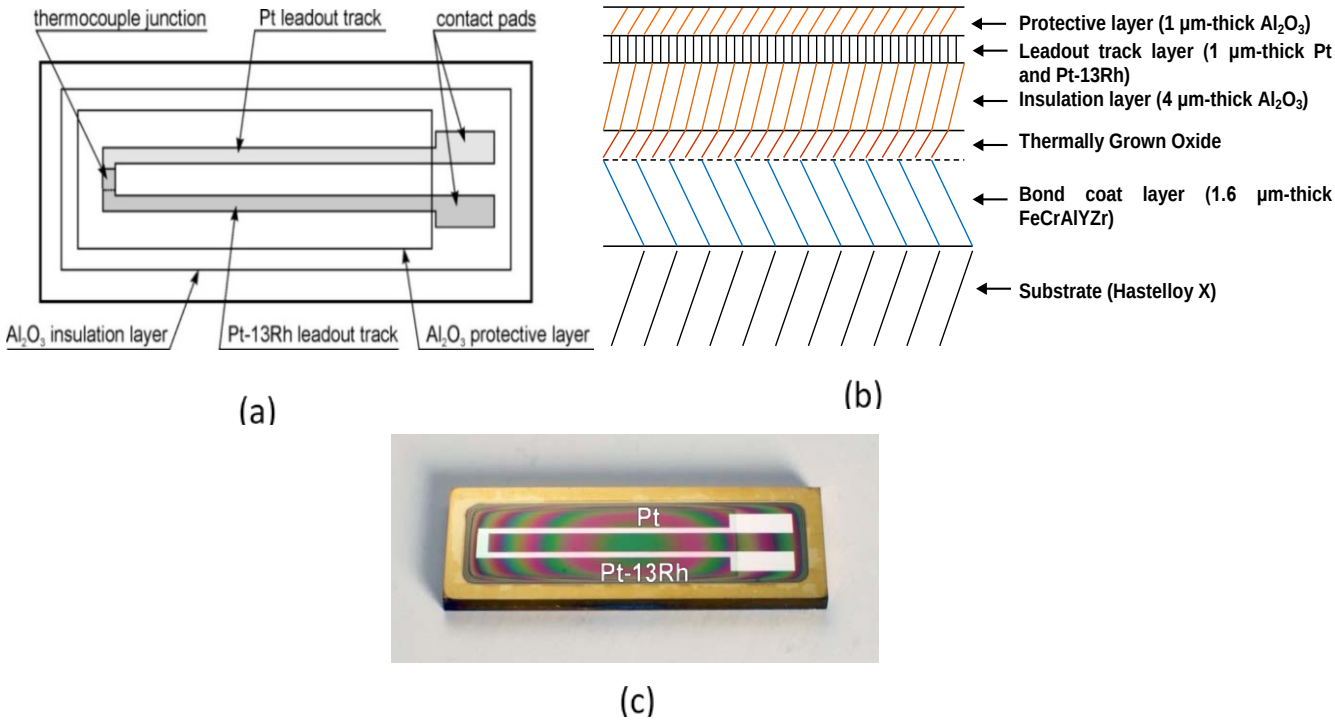

Figure 1: (a) General design of the TFTC sensor, (b) Multi-layer structure of the TFTC sensor and (c) Optical microscopy image of a TFTC sensor prepared by PLD deposition.

Table 1: Process conditions used to fabricate functional layers of the TFTC sensor.

	Target composition	Layer thickness	Deposition rate	Substrate temperature	Working gas	Working pressure	Post-deposition heat treatment
FeCrAlYZr layer	72.8Fe-22Cr-5Al-0.1Y-0.1Zr	1.6 µm	0.20 µm/h	Room temperature	None	4×10^{-7} Torr	At 600 °C for 3.5 h in 200 mTorr O_2
Insulation layer	Al_2O_3	4 µm	0.34 µm/h	600°C	Oxygen	40 mTorr	None
Pt leadout track layer #1	Pt	1 µm	0.13 µm/h	Room temperature	None	4×10^{-7} Torr	None
Pt-13Rh leadout track layer #2	Pt-13Rh	1 µm	0.13 µm/h	Room temperature	None	4×10^{-7} Torr	None
Protective layer	Al_2O_3	1 µm	0.34 µm/h	200°C	Oxygen	10 mTorr	None

Figure 2: Photograph of a custom-designed alumina fixture used for TFTC sensor durability testing.

3.0 RESULTS

3.1 Sensor characterization and durability testing

Optical microscopy analyses of as-fabricated TFTC sensor did not reveal any visible defects, cracking or spallation of the functional layers of the sensor. It was confirmed that PLD of individual layers using stenciled shadow masks fabricated by laser micromachining was effective in forming the required patterns for the Al_2O_3 insulating layer, the Pt and Pt-13Rh sensing/leadout tracks, and the Al_2O_3 protection layer. The surface profiler images showed very sharp edges of the sensing layer, indicating that the shadow mask worked well for patterning the individual layers with little materials deposited under the mask. This new method of combing PLD with laser micro-machined shadow masking can be a less expensive alternative to the conventional TFTC sensor fabrication process based on the combination of sputtering and photolithography, which is characterized by a much higher cost and a tendency for surface contamination with chemical residues or compositional changes. The PLD process is known for its ability of congruent transfer of the target composition to the coating, which ensures high reproducibility of thermoelectric properties of the fabricated TFTC sensor.

The high-temperature performance of the TFTC sensor was evaluated in ambient atmosphere. When the test temperature was lower than T_t, which was about 750°C at the beginning of testing, the sensor readings were identical to those of the S-type reference thermocouple. Exceeding T_t caused a sudden drop of the sensor output resulting in a discrepancy, δ, between the sensor output, T_{sensor} and the actual temperature, $T_{actual,}$ measured by the reference thermocouple, as shown in Fig. 3. Three interesting phenomena can be observed in the figure. First, the larger the sensor overheat, $\Delta = T_{actual} - T_t$, the larger the sensor error, δ. Second, at a fixed sensor overheat value, after the initial abrupt drop in the output, the sensor readings started recovering as if it experienced "self-healing". And third, once the test temperature, T_{actual}, measured by the reference thermocouple, was reduced to the level of T_t, the TFTC sensor output immediately restored to that of the reference thermocouple (i.e., $\delta=0$), as seen in Fig. 3 at the 110^{th} and 210^{th} minutes.

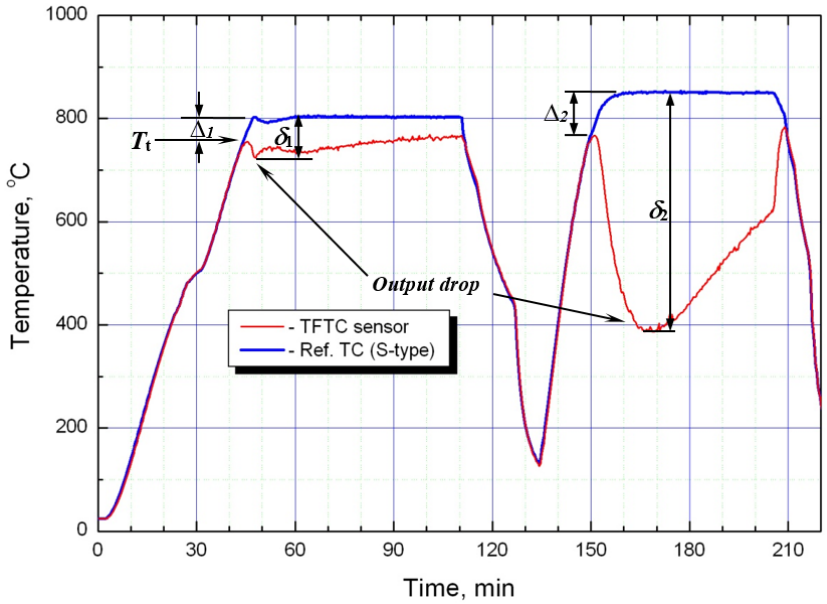

Figure 3: Temperature readings from both the TFTC sensor and the reference thermocouple during the first 220 minutes of testing.

To confirm that the observed sensor recovery was irreversible, the sensor underwent multiple thermal cycles. As illustrated in Fig. 4, this recovery effect was not only permanent, but after each thermal cycle the absolute value of T_t increased incrementally from 750°C to almost 800°C, demonstrating that the sensor could be "trained" to operate at higher temperatures as compared to its initial condition.

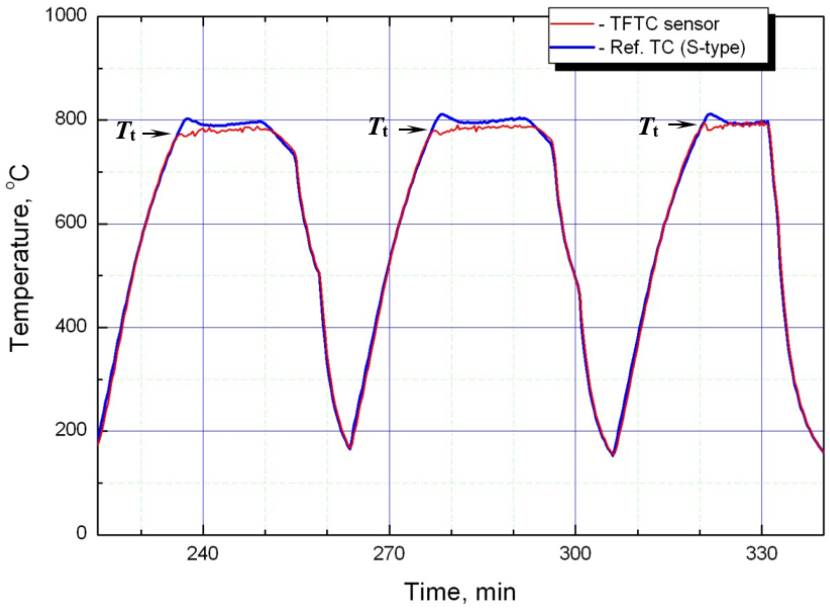

Figure 4: Temperature readings of both the TFTC sensor and the reference thermocouple during thermal cycles.

To further raise the upper limit of the sensor operating temperature, the TFTC device was exposed to 850ºC for 17.5 hours. The results presented in Fig. 5 show that it took about 10 hours at 850ºC for the sensor to equalize its output with that of the reference thermocouple. Subsequently, the sensor was capable of withstanding multiple thermal cycles while providing accurate readings at temperatures up to 800ºC. An increase in the test temperature to 900ºC did not cause the sensor failure although some discrepancy was observed between the readings of the TFTC sensor and those of the reference thermocouple at temperatures above 800ºC.

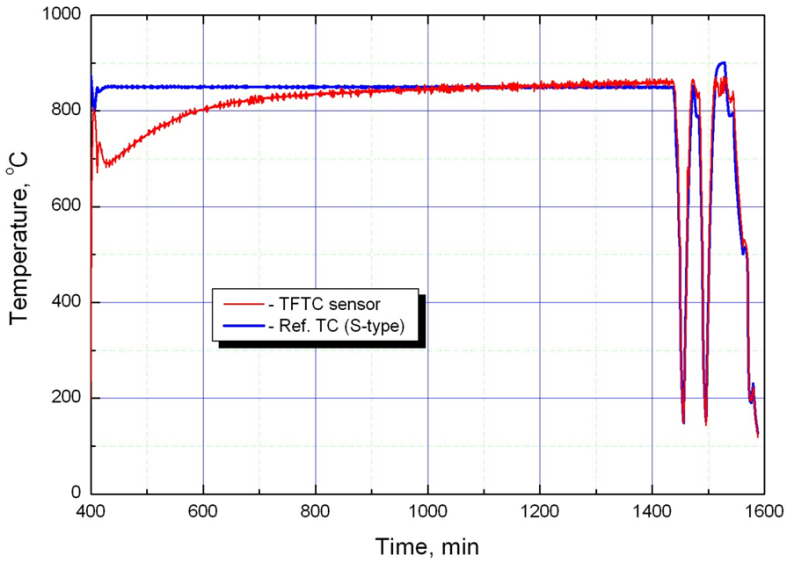

Figure 5: Temperature readings of both the TFTC sensor and the reference thermocouple during 17.5-hour training followed by thermal cycles up to 900ºC.

3.2 Analyses of the TFTC sensor after durability testing

The SEM-BSE analysis of the sensor after thermal cyclic testing (as described in Fig. 3 and 4) and isothermal testing (as described in Fig. 5) revealed that the areas occupied by the leadout tracks were covered by a network of cracks, as seen in Fig. 6 (a). Furthermore, the SEM-SE analysis presented in Fig. 6 (b) showed multiple cracks in the sensor regions occupied by the Al_2O_3 protective layer. Noticeably, the type of cracks formed within the areas occupied by Pt tracks was different from those formed in the area occupied by Pt-13Rh, as clearly shown in Fig. 6(c). The density of the cracks in this area was lower than in the areas corresponding to Pt-13Rh leadout tracks. The cracks within the Pt area appeared as thin white lines while those formed within the Pt-13Rh tracks consisted of alternating white and black lines. Fig. 6(d) depicts the crack appearance within the Pt-13Rh leadout track area acquired in the SEM-SE mode. Spot EDS analysis of these white and black crack fragments revealed that the white cracks were associated with a large content of Pt while the black ones were mainly associated with Al and O presence and a negligible amount of Pt, as seen in Table 2. The areas surrounded by cracks showed an intermediate content of Pt. Based on the SEM/EDS analyses it was suggested that the cracks formed in the TFTC sensor during durability testing could be divided in two groups depending on their depth, BSE contrast and Pt concentrations. The cracks appearing as thin white lines in the SEM-BSE micrograph (see Fig. 6(c)) and showing the presence of Pt in large quantities (see Table 2) are believed to originate from the Pt and Pt-13Rh leadout track layers exposed to the SEM electron beam through the gaps in the top Al_2O_3 protective layer (the crack labelled with “W” in Fig. 7). Pt is a heavy element and typically generates a strong SEM-BSE signal.

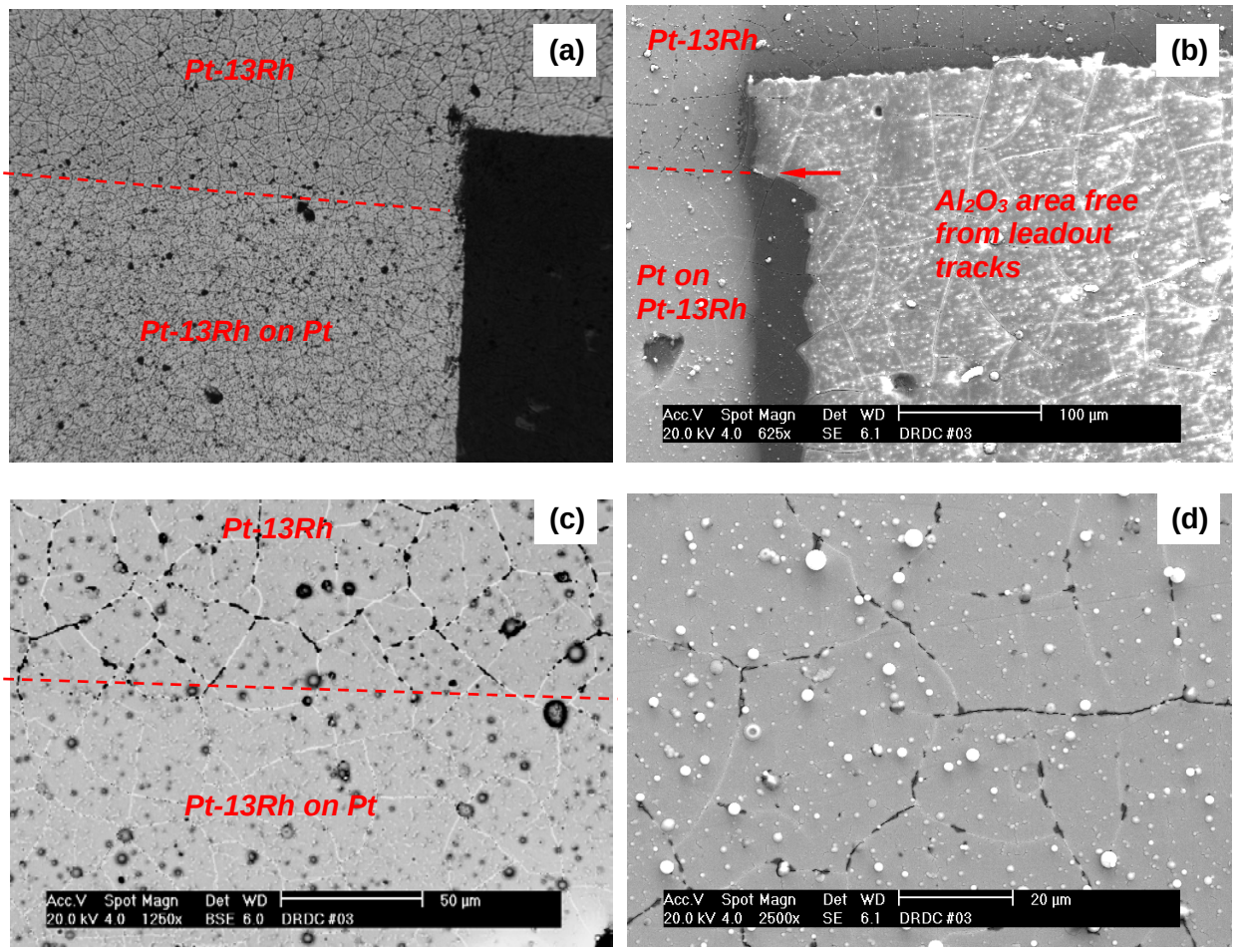

Figure 6: Surface images of the TFTC sensor within the Pt/Pt-13Rh junction (shown with a dotted line) acquired by (a) optical microscopy, (b) SEM in SE mode, and (c) SEM in BSE mode. (d) SEM-SE surface image of the sensor within the Pt-13Rh leadout track area.

Table 2. EDS surface analysis of the sensor (at. %)

	Pt	Al	O
Area surrounded by cracks	9.0	33.3	57.7
White cracks	14.8	30.1	55.1
Black cracks	1.8	45.5	52.7

According to the SEM-EDS analysis (Table 2), the cracks appearing in the SEM-BSE micrographs as black lines (Fig. 6(c) and 6(d)) are mainly associated with the presence of Al and O. These cracks are believed to be much deeper than the "W"-type ones and propagate across the thickness of both the Al_2O_3 protective layer and the Pt-13Rh layer (the crack labelled with "B" in Fig. 7). As a result, the surface of the underlying Al_2O_3 insulation layer becomes exposed to the SEM electron beam through the cracks showing high content of Al and O. As the contrast of SEM-BSE image is determined by the atomic weight of the detected elements, lighter elements such as Al and O give rise to a much darker contrast compared to heavier elements such as

Pt, which explains the “black” appearance of these cracks in the micrographs.

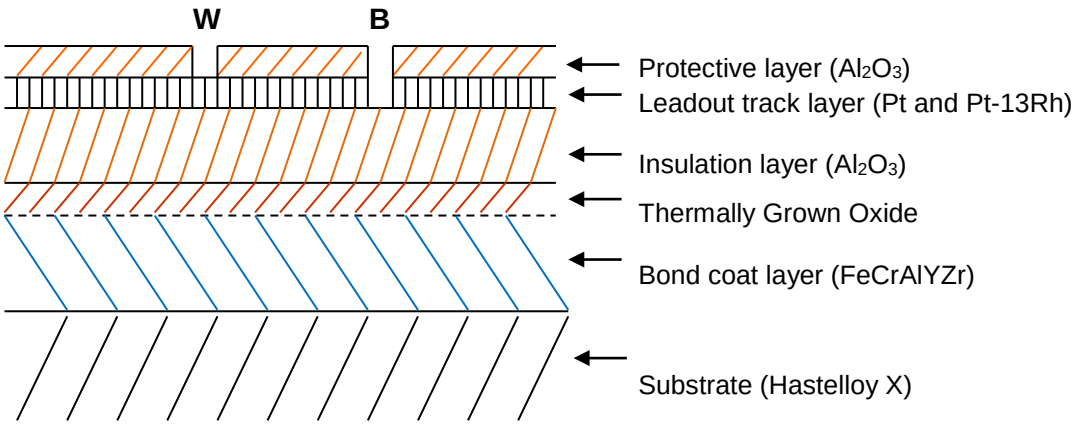

Figure 7: Schematic of the cracks formed in the multi-layered TFTC sensor.

Cracking of the top Al_2O_3 protective layer after thermal cycling tests was reported earlier for thin film strain gauges [10]. According to Godefroy *et al*. [11], the main causes of the cracking are high tensile thermal stresses built up in the alumina layer during heating because of its relatively low coefficient of thermal expansion (CTE) compared to that of the metallic substrate (see Table 3) and its low rupture strength under tensile stress. Since the cross sectional area of the Al_2O_3 layers (including both thermally grown and insulation layers) is negligible compared to the substrate, the entire tensile strain is accommodated by these layers which causes cracking.

Table 3. CTE of materials used in the TFTC sensor design (× 10^{-6} K^{-1})

Material	CTE	Reference
Al_2O_3	8.0	[11]
Pt, Pt-13Rh	~9.6	[12, 13]
FeCrAlYZr	14.8	[14]
Hastelloy X	15.1	[15]

The observed cracking of the Pt-13Rh layer could also be explained by its relatively low CTE compared to that of the Hastelloy X substrate (Table 3). However, the “W” cracks were not found in the Pt layer which has a CTE similar to that of Pt-13Rh. In fact, Pt should be more vulnerable to cracking due to its yield stress about 3 times lower than that of Pt-13Rh [12]. Therefore, further studies are required to explain the origin of Pt-13Rh cracking during thermal cycling tests and the observed higher cracking resistance of Pt film.

The main phenomena observed in the TFTC sensor during thermal cycling tests, i.e. (1) the existence of the threshold temperature T_t; (2) the fast recovery once the test temperature was reduced to the level of T_t; and (3) the slow recovery (“training”) by overheating the sensor and providing sufficient time for the sensor to restore its measurement capability, can be related to the presence of various defects in the sensor. An analysis of the sensor equivalent electric diagram presented in Fig. 8 showed that at least two types of defects could be responsible for the above phenomena. The first type of defects are discontinuities in the Pt and Pt-

13Rh leadout track layers which can increase electrical resistances of the tracks, R_1 and R_2, causing the sensor output voltage, E, to decrease. The "B" type cracks formed in the Pt-13h layer (Fig. 7) could be such discontinuities. At low temperatures the gaps in these cracks are small and do not affect the track resistance. However, when the test temperature exceeds T_t, the gaps in the Pt-13h layer widen and start affecting its electrical conductivity causing E to decrease. Once the test temperature is reduced below T_t, the gaps close up and the initial layer conductivity as well as the sensor output are restored.

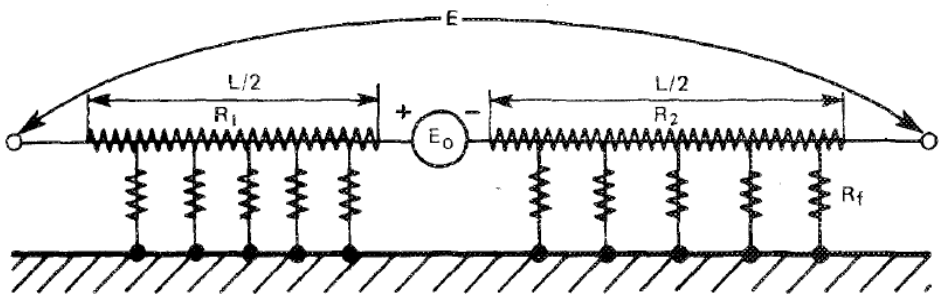

Figure 8: Equivalent electric diagram of the TFTC sensor: E_o is the electromotive force generated by the thermocouple junction, R_1 and R_2 are electrical resistances of the Pt and Pt-13h leadout tracks, respectively and R_f is the resistance of insulation between the leadout tracks and the substrate [19].

The second type of defects capable of affecting the sensor output could be micro-bridges creating short circuits between the sensing layers and the bond coat (see equivalent resistors R_f in Fig. 8). When these micro-bridges are formed on both sides of the thermocouple junction, these defects shunt the junction's electromotive force, E_o, causing the sensor's output to drop.

The formation of short-circuiting defects in thin film sensors was reported before [13]. The exact nature of these defects in TFTC sensors is not yet understood. However, the presence of the FeCrAlYZr bond coat on the substrate surface and its ability to form a thermally grown oxide (TGO) layer when exposed to high temperatures in air are believed to be the main reasons for the observed slow recovery ("training") phenomenon. The self-healing ability of TGO layers formed on the surface of Al-containing metallic surfaces is a well-known phenomenon in gas turbine materials research [14].

4.0 CONCLUSIONS

Multilayer thin film thermocouple sensors consisting of a FeCrAlYZr bond layer, an insulating (Al_2O_3) layer, a sensing (Pt and Pt-13Rh) layer and a protective (Al_2O_3) layer have been successfully fabricated on Hastelloy X superalloy substrates by Pulsed Laser Deposition and patterning with laser micro-machined shadow masks. This new "dry" fabrication approach allows for excellent control of the chemical composition and physical characteristics of the constituent layers and their interfaces, thus achieving good film uniformity and adhesion to the substrate. The results of limited atmospheric thermal cyclic testing of a TFTC sensor produced by the described approach demonstrated that the PLD method can be used to fabricate TFTC sensors at substrate temperatures not exceeding 600°C that are fully functional at temperatures up to 750°C. Analyses of the sensor performance during thermal cyclic testing revealed a number of phenomena including: (i) the existence of a threshold temperature below which precise temperature measurement was achieved; (ii) an abrupt drop in the sensor output occurring when the sensor temperature exceeded the threshold value, with a fast recovery of the sensor output once the temperature was

reduced below the threshold level; (iii) sensor “training” capable of increasing the threshold temperature through exposure of the device to the above-the-threshold temperatures. These phenomena were explained by the presence of various defects and structural changes in the functional layers of the TFTC sensor during thermal cycling tests. The thermal cyclic durability testing of the TFTC sensors conducted in this study was performed without applying mechanical loading. The main objective was to evaluate the compatibility of constituent layers, the ability of pulsed laser deposition to produce high quality functional layers of TFTC sensors, and the stability of the fabricated multi-layered TFTC device in a thermal cyclic environment. Adding mechanical loads represents a more severe test condition, and is considered for the next evaluation work.

[1] R.C. Budhani, S. Prakash, and R.F. Bunshah, Thin-film temperature sensors for gas turbine engines: Problems and prospects, J. Vac. Sci. Technol. A 4 (1986) 2609-2617.

[2] J.-F. Lei and H.A. Will, Thin-film thermocouples and strain-gauge technologies for engine applications, Sensors and Actuators A 65 (1998) 187-193.

[3] L.C. Martin and R. Holanada, Applications of Thin Film Thermocouples for Surface Temperature Measurement, NASA Report No TM-106714, 1994.

[4] M. Zielinski, Development of thin-film sensors directly applied to aero-engine components (THIN FILM SENSORS), in Advances in Techniques for Engine Applications Edited by R. Dunker, John Wiley & Sons Ltd., 1995.

[5] H.P. Grant, J.S. Przybyszewski, and R.G. Claing, Turbine blade temperature measurements using thin film temperature sensors, NASA Report No 81-19277, April 1981.

[6] L.R. Zhao, Q. Yang, D. Morphy, D. Yang, S. Lee and S. Nikumb, "Fabrication and demonstration of high temperature thin film sensors for gas turbines – 1st annual report", LTR-SMPL-2008-0096, May 2008.

[7] L.R. Zhao, Q. Yang, D. Yang and S. Lee, "Fabrication and demonstration of high temperature thin film sensors for gas turbines – 2nd annual report", LTR-SMPL-2009-0074, April 2009.

[8] L.R. Zhao, V. Pankov, W. Chen, D. Yang, B. Gibson, A. Bugg and N. Mrad, "Fabrication and demonstration of high temperature thin film sensors for gas turbines – 3rd annual report", LTR-SMPL-2010-0072, April 2010.

[9] L.R. Zhao, D. Yang, and N. Mrad, "High Temperature Blade Assessment – Progress Report", LM-SMPL-2011-0067

[10] C.O. Hulse et al., High temperature static strain gage development, NASA Lewis Research Center, Report CR-189044, August 1991.

[11] J.C. Godefroy et al., Thin film temperature heat fluxometers, Thin Solid Films 193-194 (1990) 924-934

[12] B. Fischer, High temperature mechanical properties of the platinum group metals: Stress-rupture strength and creep behaviour at extremely high temperatures, Platinum Metals Rev. 43 (1999) 18-28.

[13] J.P. Grant et al., Thin film strain gage development program, NASA Lewis Research Center, NASA Report CR-174707, December 1983.

[14] K.G. Kreider, Thin film thermocouples for internal combustion engines, J. Vac. Sci. Technol. A 4 (1986) 2618-2623.